Antagonistic Pump With Multiple Pumping Modes for On-Demand Soft Robot Actuation and Control

Jianshu Zhou, *Member, IEEE*, Wei Chen, Hanwen Cao, *Graduate Student Member, IEEE*, Qiguang He, and Yunhui Liu, *Fellow, IEEE*

***Abstract*—Pneumatic soft robots are prized for their flexibility in achieving adaptable deformations and compliance adjustments. However, the conventional pumps used in these systems often rely on simplistic, sensorless, and ON–OFF control mechanisms, which limit the potential of these robots. Drawing inspiration from the intricate functionality of the natural heart-pumping mechanism, we present an innovative and versatile pump that integrates an antagonistic pumping mechanism with a reinforcement-learning-powered control strategy. The antagonistic pump features dual chambers for expansion and deflation, valve-controlled interconnections, and distributed pressure sensors. This dedicated architecture enables a nuanced air exchange logic and pumping sequence, thereby facilitating a wide range of pneumatic actuation possibilities for pneumatic soft robots. Our pressure control method leverages the structural capabilities and degrees of freedom inherent in the pump, enhancing pumping efficiency and precision. Diverging from the traditional controllers, it autonomously evaluates the properties of unknown connected loads and dynamically adjusts pumping actions accordingly. Consequently, the pump provides multiple pumping modes, including load perception, rapid inflation, dual-load control, adaptive pumping across positive and negative pressure ranges, fine-tuning, and instantaneous pressure switching. Moreover, by iteratively executing the pumping cycle, the pump can extend its output pressure limits. We have successfully built and tested a prototype pump, validating its ability to achieve a broad range of pressures with precise and robust control. These results underscore the pump's potential to actuate diverse soft robots through multimode pumping, offering a pioneering solution for universal soft robot actuation and control.**

***Index Terms*—Intelligent system, pneumatic actuation, reinforcement learning, soft robotics.**

I. Introduction

PNEUMATIC soft robots have garnered significant attention in academic and engineering domains due to their remarkable performance in applications that necessitate compliance, adaptability, and dexterity [1], [2], [3], [4]. Ensuring effective pneumatic actuation and control is crucial for enhancing task performance and facilitating safe interactions of soft robots while minimizing reliance on accurate sensing and computational costs [5], [6].

Diverse soft robot designs demand distinct actuation methods. For instance, traditional industrial pumps [7], such as piston pumps, with simple binary pneumatic control can accomplish ON–OFF control of pneumatic pressure, which suffices most soft grippers in pick-and-place scenarios. However, more complex soft robots, such as grippers for in-hand manipulation or locomotion robots, necessitate precise pneumatic pressure perception and flexible pressure adjustments to accomplish specialized movements [8]. Traditional pumps often have limited pumping modes and, therefore, have difficulties in such cases.

Moreover, various soft robots can be constructed using different elastic materials with varying actuation chamber sizes. Incorporating knowledge of these models as priors can enhance pressure control performance by predicting the specific effect of control actions on the target robots. However, the conventional pressure controllers typically employ a uniform control strategy for all soft robots, neglecting the unique characteristics of individual soft robot models.

Consequently, there arises a need for a pneumatic pump capable of achieving multiple pumping modes and employing adaptive and antagonistic pumping strategies tailored to diverse soft robots and target pressure profiles.

Nature offers intriguing examples of specialized pumping mechanisms that have evolved in various biological organs to facilitate circulation and regulate pressure. Among these, the circulatory systems of animals stand out as quintessential

Manuscript received 17 July 2023; revised 8 October 2023; accepted 3 December 2023. Recommended by Technical Editor H. Zhang and Senior Editor K. Oldham. This work was supported in part by the Shenzhen Portion of Shenzhen–Hong Kong Science and Technology Innovation Cooperation Zone (No. HZOBKCZYB 20200089), in part by the CUHK T Stone Robotics Institute InnoHK of the Government of the Hong Kong Special Administrative Region via the Hong Kong Centre for Logistics Robotics, and in part by the Research Grants Council of Hong Kong under Grant 14207320 and Grant 14207423. *(Corresponding authors: Qiguang He; Yunhui Liu.)*

Jianshu Zhou and Yunhui Liu are with the Department of Mechanical and Automation Engineering, Chinese University of Hong Kong, Hong Kong, and also with the Hong Kong Centre for Logistics Robotics, Hong Kong (e-mail: jianshuzhou@cuhk.edu.hk; yhliu@cuhk.edu.hk).

Wei Chen, Hanwen Cao, and Qiguang He are with the Department of Mechanical and Automation Engineering, Chinese University of Hong Kong, Hong Kong (e-mail: weichen@link.cuhk.edu.hk; hwcao@mae.cuhk.edu.hk; qghe@mae.cuhk.edu.hk).

This article has supplementary material provided by the authors and color versions of one or more figures available at https://doi.org/10.1109/TMECH.2023.3339814.

Digital Object Identifier 10.1109/TMECH.2023.3339814

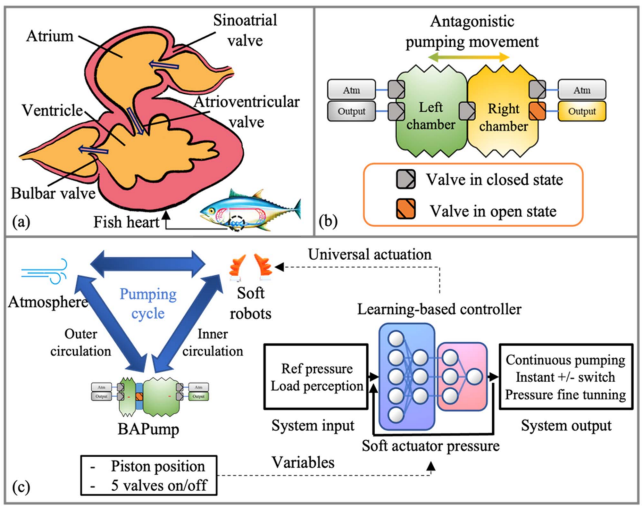

Fig. 1. Overview of the bioinspired antagonistic pump and its learning-based control strategy. (a) Typical two-chamber (atrium and ventricle) fish heat. (b) Antagonistic pump contains five valves and two chambers. (c) Pump operates through a programmable pumping cycle. Each chamber can alternate between being a compression chamber and a reservoir, which provides multiple pumping modes based on reinforcement learning.

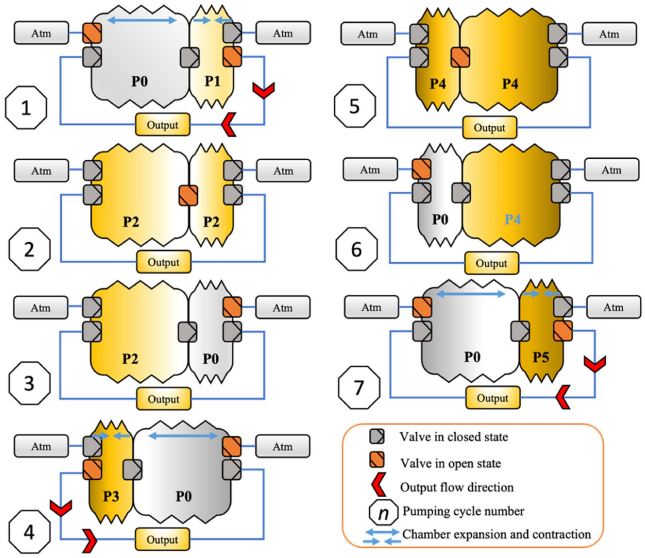

Fig. 2. Typical positive pressure pumping cycle with seven steps. "Atm" represents the atmosphere, and "output" represents the pneumatic loads, such as soft robot actuators.

biopumping systems [9]. In this context, both mollusks [10] and fish [11] feature two-chambered hearts, comprising an atrium and a ventricle [see Fig. 1(a)]. Conversely, vertebrates [12] boast multichambered hearts, including two atria and one or two ventricles [13]. This atrium-to-ventricle configuration is a recurring theme across diverse animal species, regardless of their size and habitat. Within this structural framework, the atrium acts as a reservoir for receiving blood, while the ventricle propels blood outward at precisely controlled pressures. This fundamental architecture offers inherent advantages for ensuring efficient circulation.

We draw inspiration from these natural pumping mechanisms, focusing particularly on two-chambered hearts achieving complete inner body circulation, such as the fish heart as an illustrative example. A typical fish heart connects its atrium and ventricle through an atrioventricular valve [see Fig. 1(a)], which meticulously regulates blood flow. In addition, the sinoatrial valve at the atrium's inlet and the bulbar valve at the ventricle's outlet [see Fig. 1(a)] play crucial roles in this process. To elucidate the fish heart's operation, when muscle bundles contract, the atrium's volume decreases, prompting blood to flow from the atrium to the ventricle via the atrioventricular valve. However, natural two-chamber hearts are usually limited to unidirectional pumping without negative pressure capabilities or pressure regulation, which is not desirable for soft robot applications.

Expanding upon the natural two-chamber heart mechanism, we propose a bioinspired antagonistic pump that inherits the natural pumping efficacy and enhances the overall performance. The antagonistic pump consists of a pair of soft actuators interconnected via valves and monitored using distributed pressure sensors, employing a two-chambers-and-five-valves structure [see Fig. 1(b)]. This design maintains an inner circulation and incorporates an outer circulation of air [see Fig. 1(c)]. Each chamber can alternate between being a compression chamber and a reservoir. This is achieved by compressing gas in one chamber, while the other serves as a reservoir for the compressed gas. Subsequently, their roles switch, with the former compression chamber becoming the standby reservoir and vice-versa. This repetitive process incrementally increases or decreases chamber pressure. Before equalizing the pressure of a chamber with the pneumatic load, the output chamber's pressure is preadjusted to a desired value. A typical cyclic process with seven steps for a continuous positive pressure output is illustrated in Fig. 2.

Antagonistic pump embodies three distinct characteristics that confer significant advantages over the conventional pumps. First, through the iterative repetition of this cycle, the pump achieves progressively higher pressure limits. Each successive iteration of the pumping cycle consistently attains greater pressure thresholds than its predecessor. Second, the process demonstrates symmetrical versatility with respect to directionality. Both chambers are capable of functioning as either compression chambers or reservoirs, affording the flexibility for both chambers to serve as output chambers. In extreme scenarios, the antagonistic pump can intelligently assign roles to the two chambers, enabling it to control two pneumatic loads simultaneously. Third, the pump has the unique capability to generate either positive or negative pressure, contingent on whether the chambers are compressing or expanding. This adaptability allows the pump to effectively track complex pressure curves. Collectively, these advantages endow the pump with multiple pumping modes, rendering it well suited for actuating a diverse range of soft robots.

To govern the output pressure, we have introduced a reinforcement-learning-based controller that accurately predicts the subsequent pumping actions, such as chamber expansion or

deflation, and valve opening or closing based on the current pump and load pressure. By executing a sequence of actions in a predefined order, the controller can effectively and efficiently adjust the pressure to the desired value [see Fig. 1(c)], leveraging the pump's degree of freedom and sensing capabilities. This imbues the pump with the intelligence required for flexible pumping movements and robust pressure control, distinguishing it from traditional industrial pumps. In addition, we developed an interactive load context perception method to automatically adapt to different types of soft robots without prior knowledge of their specific characteristics. By discerning the essential traits of the soft robots being actuated, the pump can rapidly adapt to previously unseen soft robots with varying chamber sizes and stiffness in a few steps. The proposed learning method can be trained entirely in simulation and seamlessly transferred to the real world without physical demonstrations or training. A prototype of the bioinspired antagonistic pump has been successfully applied to several typical robotic applications that demand versatile pumping. The contributions of this work can be summarized as follows.

1) Introducing an antagonistic pump that encompasses multiple pumping modes, including unknown load perception, rapid inflation, double-load control, adaptive pumping across positive and negative pressure ranges, precise fine-tuning, and instant pressure switches. By programmable repeating the pumping cycles, the output pressure limits can be adjusted.
2) Proposing an on-demand pressure control method that intelligently determines the appropriate pumping actions for different soft robots based on reinforcement learning.

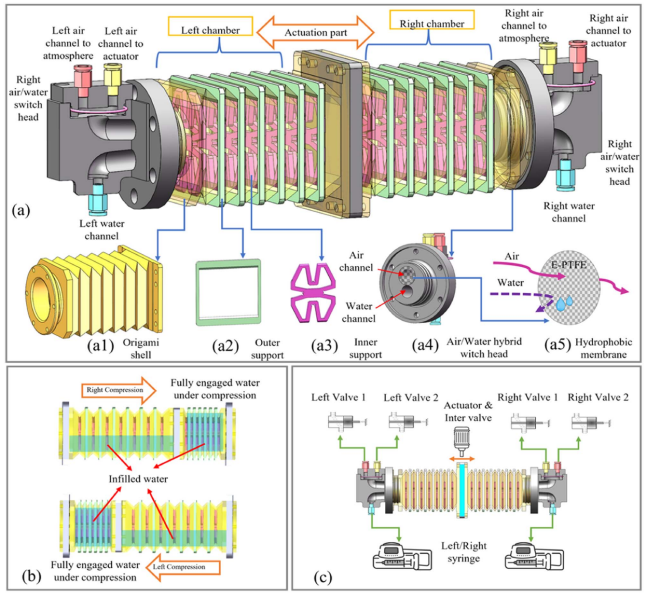

Fig. 3. Antagonistic pump designs. (a) Schematic diagram of the pump. The pump is composed of a pair of antagonistic origami chambers, chamber supports, and switch heads with hydrophobic membrane. (b) Origami chambers can expand and contract. Pneumatic pressure in the left and right chambers can be changed simultaneously by the antagonistic movement. The amount of liquid filled inside the chambers can adjust the upper and lower bounds of the pressure output range. (c) Schematic of the gas connections for the pump. The syringes are employed for liquid infilling.

II. Bioinspired Design

A. Antagonistic Pumping Mechanism and Antagonistic Pump Design

The heart, a vital organ in numerous animal species, drives blood throughout their bodies. Cardiac chamber configurations, essential for this function, vary across the animal kingdom [14]. Arthropods have a basic single-chambered heart, providing rudimentary pumping [15]. In contrast, mollusks and fishes have a more advanced two-chambered heart, comprising a ventricle and an atrium [16]. Mammals, birds, amphibians, and reptiles possess complex multichambered hearts, vital for maintaining body temperature [17]. These cardiac designs share a fundamental atrium–ventricle framework, regulating blood pressure. In this structure, chambers have specialized roles: the atrium collects oxygenated blood, buffering venous return from ejection, while the ventricle propels it into the body.

Cardiac muscles and valves are critical [18], [19]. During diastole, atrial and ventricular muscle relaxation coincides with the opening of the sinoatrial valve, allowing blood inflow, and replenishing the atrium. Atrial contraction propels blood into the ventricle, aided by the atrioventricular valve, which prevents backflow. In systole, vigorous ventricular muscle contraction opens the bulbar valve, facilitating blood ejection. It is indicated that two-chamber or multichamber structures have better control over fluid pressure and flow rate than the single-chamber structure. A typical fish heart has a two-chambered design, complemented by three valves, maintaining inner blood circulation and optimal pressure [see Fig. 1(a)].

While natural heart pumping excels at providing pressure for inner body circulation, it faces limitations in adapting to soft robot actuation needs, such as multidirectional actuation, negative pressure actuation, and precise pressure adjustment. The antagonistic driving mechanism, known for its effectiveness in force and stiffness actuation, offers a promising solution for addressing these pressure actuation challenges. By configuring the two chambers in an antagonistic manner, we enable them to mutually pump and finely tune the desired pressure output, as depicted in Fig. 1(b). Each chamber can seamlessly switch between acting as an actuation chamber and serving as a reservoir. When a chamber expands, it can draw in air, generating negative pressure; conversely, when the chamber compresses, it expels air to produce positive pressure. We term this innovative mechanism the "antagonistic pumping mechanism."

However, directly copying the cardiac muscles in artificial pump design is challenging due to fabrication limitations. And soft robot actuation usually requires more versatile control of fluid pressure than animal bodies. Past research found that origami actuators can guarantee safe and forceful interaction in soft robots. It has been shown that origami actuators can withstand significant pneumatic pressure (positive and negative). Therefore, instead of directly copying cardiac muscles, our pump design adopts another actuation method suitable for soft robot actuation (see Fig. 3). Each chamber is a linear origami

actuator with a free and fixed end. Two free ends are connected through a moveable part. When it moves to the left or right, both chambers' volumes change simultaneously, while the total volume of the two chambers remains almost constant.

Besides cardiac structure, we learn from animal hearts that cardiac muscles and valves are equally important. Because cardiac muscle contraction and relaxation cause fluid to flow in and out of the heart, and cardiac valves direct fluid to the correct chambers and control the inlet and outlet of the heart [19]. More importantly, the heart cannot function without the close cooperation between the actions of cardiac muscles and valves. In each cardiac cycle, the blood flows in the desired direction with the help of the opening or closing of exact cardiac valves [19]. The blood maintains proper pressure, thanks to the exact muscle actions. Different from the fish heart's two-chambers-and-three-valves structure, we take a step further and introduce a novel and more flexible two-chambers-and-five-valves structure to include the air exchange with the atmosphere, as shown in Fig. 1(c). Specifically, we set a solenoid valve that connects two chambers of the pump, two solenoid valves at the inlets of both chambers that control the connectivity between chambers and atmosphere, and two valves at the outlets that control the connectivity between chambers and pneumatic loads. This improvement allows the pump to maintain not only an inner circulation but also an outer circulation of air. For state sensing, distributed pressure sensors are placed inside the pump chambers and the outlets.

In total, the pump has five valves and a moveable part that can be actively controlled. We denote the state space as $S = \{s|s = [v_1, v_2, v_3, v_4, v_5, p]\}$, where $v_j = 0$ for valve close and $v_j = 1$ for valve open, and p is the continuous position of the moveable part. Let $A = \{a|a : s \rightarrow s'\}$ be the action space, where a is the pumping action. Thus, unlike related works with only one or two states, the antagonistic pump has versatile pumping actions. These pumping actions involve complex air exchange among the atmosphere, the pump, and soft robots being actuated through a unique pumping cycle.

Due to the nature of complex air exchange in the pump and discrete action space, it would be challenging for traditional control methods, such as the proportional-integral-derivative (PID) [20] and model predictive control (MPC) [21], to control the output pressure of the pump. Besides, an unknown pneumatic load will increase the difficulty of precise pressure control. The antagonistic pump and pneumatic loads are hard to precisely model for control because both are deformable. Toward developing a robust and accurate control strategy that can handle multiple local optima in the objective function and unknown load, we designed a novel pressure controller based on the reinforcement learning.

B. Antagonistic Pump Fabrication

Origami actuator consists of discrete facets and creases, where different crease patterns result in different morphologies and functions when folded. The origami actuators exhibit inherent compliance compared with the conventional rigid counterparts and significant strength compared with purely soft counterparts. Therefore, the origami actuator can bear large pressure and maintain interaction safety, which is desired for soft robot actuation. Therefore, we use the origami actuators as the pump chambers. Among various patterns, we chose the accordion pattern (also known as the triangular fold pattern) [22] to design our chamber [see Fig. 3(a)], for a large extension and compression ratio. The valley of the folding feature can be raised and lowered, and the mountainous feature is fixed. The body has a rectangular profile with customizable parameters. The body of the chamber can be easily scaled up for different applications.

In order to accommodate a wide range of soft robots with various applications, the pump is supposed to have customizable upper and lower pressure bounds. This is realized by the liquid infilling technique [see Fig. 3(b)]. Namely, we infill customizable amounts of liquid into both chambers, and the remaining chamber volume not occupied by the filling is valid for pumping gas. The infilled liquid is sealed by a hydrophobic membrane that allows gas to pass but stops liquid. In this way, the upper and lower pressure bounds of the pump can be controlled by the infilling volume. The overall schematic of the gas connections is given in Fig. 3(c).

We fabricate the prototype chambers with a three-dimensional printer using thermoplastic polyurethane materials (hardness = 83 A) at a temperature of 220 °C (nozzle size = 0.2 mm; layer thickness = 0.1 mm; shell thickness = 1.5 mm; printing speed = 30 mm/s; and print infill density = 100%). Furthermore, to prevent buckling, we add supporting ribs inside and outside the chambers [see Fig. 3(a)]. The supporting ribs are specially designed so that the chambers can deform along the axial direction while keeping stiff in other directions. The hydrophobic membrane is made of expandable polytetrafluoroethylene, allowing air to pass through and hinder water flowing outside of the chamber.

C. Comparison With Conventional Pump Designs

Typically, conventional pumps, such as piston pumps and diaphragm pumps, only have one chamber for gas compression [23]. This causes a significant limitation that single-chamber pumps only blow out gas on one piston stroke, i.e., they blow gas when the stroke is in one direction and refill the chamber in the other direction. However, the proposed pump can blow out gas on both strokes of chamber movements (see Fig. 2). Therefore, it blows a stronger and more constant blast than typical single-chamber pumps.

For constant blast, double-acting pumps have been proposed [24], [25], featuring two chambers and can expel gas during both strokes. However, double-acting pumps have limited and constant maximum positive and negative output pressure (MOP) throughout every pumping cycle due to their inability to transfer gas between the two chambers. The MOP is strictly determined by the ratio of the maximum chamber volume during expansion to the minimum chamber volume during compression, which means MOP can only be increased by building a larger pump if the minimum compression volume is not changeable. In contrast, thanks to the fish heart-inspired structure, each chamber of the proposed pump can function as a compression chamber

or a reservoir. By transferring gas between two chambers, the proposed pump has greater MOP during subsequent pumping cycles, as confirmed in the experimental analysis. This transferring gas is achieved by intelligently controlling the inner valve action and the corresponding chamber movements using reinforcement learning. Since the actual chamber volume does not strictly constrain the MOP of the proposed pump, it can achieve larger MOP by repeating the pumping cycles even with small-sized chambers, which offers potential advantages for miniaturized robots/pumps' applications.

III. Modeling

Our goal is to achieve versatile pumping for soft robot actuation. Namely, it can generate continuous positive/negative (+/−) output, instant +/− switch, accurate pressure adjustment, and adaptation to various soft robot actuators. Compared with industrial pumps that can only output constant and stable pressure or pneumatic flow, versatile pumping enables soft robots to perform more complex tasks that require not only constant pneumatic output. For example, versatile pumping can output positive pressure in one chamber and negative pressure in the other chamber simultaneously, which can actuate one joint of a soft manipulator to rotate in the positive direction and another joint in the negative direction. Although the design of the pump provides the possibility of versatile pumping theoretically, it is not trivial to control the pump to actually realize it. The reasons are fourfold. First, the pump has multiple degrees of freedom. This results in a high-dimensional action and state space, which is complex to control. Furthermore, there are correlations between the different degrees of freedom. For example, the moveable part's movement causes an increase in the difference between two-chamber pressure, while the opening of the internal valve results in an opposite effect. Second, like its natural counterparts, the pump can naturally pump periodically. However, the state transitions between cycles are recurrent, meaning the initial state of the next cycle always depends on the end state of the previous cycle. Although traditional controllers can control the pump inside one cycle, they cannot handle pumping states and actions in different cycles. Third, since our goal is universal soft robot actuation, the pump must accommodate various soft robot actuators with different sizes and softness. These different parameters of pneumatic loads will affect the optimal pumping behavior of the pump. Fourth, the accurate dynamic modeling of the chambers and loads is challenging. All four reasons challenge traditional controllers that are usually used in pumps. To solve this complex control problem, we first derive an analytical model of the pump and then design a pneumatic controller that can learn optimal pumping actions by itself in the real world and simulation based on the derived model.

The cross section of the origami actuator [the orange mask in Fig. 4(b)] is a rectangle. Its area varies at different cross-sectional heights h due to the geometry pattern of the origami actuator

$$S = (a+2d)\left[a+\left(\sqrt{2}c-2d\right)\sqrt{1-\frac{2h_y^2}{c^2}}\right] \tag{1}$$

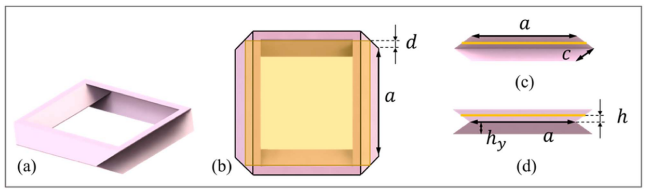

Fig. 4. Analytical modeling of the pump chamber. (a) One layer of the chamber. (b) Top view of one layer of the chamber. (c) Right-side view of one layer of the chamber. (d) Left-side view of one layer of the chamber.

where a is the constant, and d is determined by

$$d = \frac{\sqrt{2}}{2}c\left(1-\frac{h}{h_y}\right). \tag{2}$$

Combining (1) and (2), we obtain the volume of a layer

$$V_y = 2\int_0^{h_y} S(h)\,dh = 2a^2h_y + \sqrt{2}ach_y + \left(\sqrt{2}c-\frac{2}{3}a\right)h_y\sqrt{c^2-2h_y^2}. \tag{3}$$

An origami actuator chamber is composed of m layers. When the chamber length L is changed by the motor, the length of every layer changes according to $L_y = L/m = 2h_y$, assuming that the chamber deformation is uniform along the axial direction. Therefore, the chamber volume can be written as follows:

$$V_c = mV_y - V_s - V_f \tag{4}$$

where V_s is the volume of supporting ribs inside the origami actuator and V_f is the volume of liquid infilling.

To calculate the pressure, assume adiabatic ideal gas

$$PV = nRT \tag{5}$$

where n is the number of moles, R is the ideal gas constant, and T is the absolute temperature.

To model the elastics of loads, we assume that the load volume could be approximated by $V_l^t = V_l^0 + \frac{P_l^t - P_0}{P_0}C_d$ for both loads, where V_l^0 is the volume at atmosphere pressure and C_d describes the material elastic.

Let P_{cL} and P_{cR} be the left and right chamber pressures. Each pumping action results in a transition in the pump state

$$v_1 = 0 \to 1: \; P_{cL}^{t+1} = P_0 \tag{6}$$

$$v_2 = 0 \to 1: \; P_{cR}^{t+1} = P_0 \tag{7}$$

$$v_3 = 0 \to 1: \; P_{cL}^{t+1} = P_{cR}^{t+1} = \frac{V_{cL}^t P_{cL}^t + V_{cR}^t P_{cR}^t}{V_{cL}^t + V_{cR}^t} \tag{8}$$

$$v_4 = 0 \to 1: \; P_{cL}^{t+1} = P_{lL}^{t+1} \tag{9}$$

$$v_5 = 0 \to 1: \; P_{cR}^{t+1} = P_{lR}^{t+1} \tag{10}$$

$$p = p^t \to p^{t+1}: \; P_{cL}^{t+1} = \frac{V_{cL}^t}{V_{cL}^{t+1}}P_{cL}^t, \; P_{cR}^{t+1} = \frac{V_{cR}^t}{V_{cR}^{t+1}}P_{cR}^t \tag{11}$$

where P_{lL}^{t+1} and P_{lR}^{t+1} can be determined by

$$P_c V_c + P_l \left(V_l^0 + \frac{P_l^t - P_0}{P_0} C_d \right) = P_l^{t+1} V_c + P_l^{t+1} \left(V_l^0 + \frac{P_l^{t+1} - P_0}{P_0} C_d \right). \tag{12}$$

Here, we assume that the changes in V_{cL} or V_{cR} is neglectable compared with the changes in V_{lL} and V_{lR} during $(t,\ t+1)$. In our implementation, $h_y = 4$ mm, $a = 34$ mm, $c = 6.8$ mm, and $m = 6$.

Fig. 2 shows some examples of pumping cycles of the soft pump for generating positive and negative pressure. Repeating the cycles, the soft pump can generate higher positive or lower negative pressure. To calculate the extreme pressure that the soft pump can attain after pumping, assuming adiabatic ideal gas

$$PV = nRT \tag{13}$$

where n is the number of moles, R is the ideal gas constant, and T is the absolute temperature. In the first type of state transition

$$P_2 = \frac{V_1}{V_{\max}} P_1 \tag{14}$$

$$P_4 = \frac{V_{\min}}{V_{\max}} P_3. \tag{15}$$

In the second type of state transition

$$P_3 = \frac{V_{\min} P_0 + V_{\max} P_2}{V} \tag{16}$$

$$P_5 = \frac{V_{\min} P_0 + V_{\max} P_4}{V} \tag{17}$$

where $V = V_{\min} + V_{\max}$. A general formula of negative pressure can be deducted as

$$P_{2n+1} = \sum_{i=1}^{n} \frac{V_{\min}^i}{V^i} P_0 + \frac{V_1 V_{\min}^{n-1}}{V^n} P_1 \tag{18}$$

$$P_{2n} = \sum_{i=1}^{n} \frac{V_{\min}^{i+1}}{V_{\max} V^i} P_0 + \frac{V_1 V_{\min}^n}{V_{\max} V^n} P_1. \tag{19}$$

The lower bounds of negative pressure are derived by finding the limits

$$\lim_{n\to\infty} P_{2n+1} = \frac{V_{\min}}{V_{\max}} P_1 \tag{20}$$

$$\lim_{n\to\infty} P_{2n} = \frac{V_{\min}^2}{V_{\max}^2} P_1. \tag{21}$$

The movement trajectory of generating positive pressure is similar to generating negative pressure. Therefore, we can obtain the general formula of positive pressure as

$$P_{2n+1} = \sum_{i=1}^{n} \frac{V_{\max}^i}{V^i} P_0 + \frac{V_1 V_{\max}^{n-1}}{V^n} P_1 \tag{22}$$

$$P_{2n} = \sum_{i=1}^{n} \frac{V_{\max}^{i+1}}{V_{\min} V^i} P_0 + \frac{V_1 V_{\max}^n}{V_{\min} V^n} P_1. \tag{23}$$

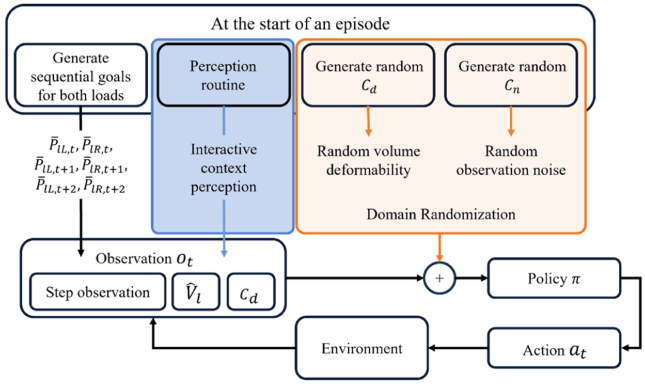

Fig. 5. Reinforcement-learning framework. At the start of each episode, the agent attempts to acquire the load context by interactive perception, and a random domain is created. The obtained load context is formulated as parts of the observation, which facilitates generalization to various unknown and unseen pneumatic loads. The pressure goals of the current and two future timesteps are provided to the agent. The agent then makes decisions on the action based on the observation. The chosen action will be executed and the pressure of the pump and/or the loads will be changed.

The theoretical upper bounds of positive pressure are derived by finding the limits

$$\lim_{n\to\infty} P_{2n+1} = \frac{V_{\max}}{V_{\min}} P_1 \tag{24}$$

$$\lim_{n\to\infty} P_{2n} = \frac{V_{\max}^2}{V_{\min}^2} P_1. \tag{25}$$

IV. Pressure Control

A. Problem Formulation

The problem is formulated as a Markov decision process [26] characterized by observations, actions, and rewards. At every step, the agent (i.e., the antagonistic pump) perceives an observation o_t and then decides on an action a_t to execute according to a policy $\pi(o_t)$. A reward signal r_t will be received upon a_t execution. The goal of the agent is to maximize its cumulative reward (return), given by $R = \sum_{t=0}^{\infty} \gamma^t r_t$, where γ is a discount factor. The overall learning framework is shown in Fig. 5.

1) Observations: Step observations at discrete timesteps are defined as the valve states, moveable part position, length of chambers, the pressure of both chambers, pressure of both loads, target pressure of both loads of current timestep and two future timesteps, and the estimated volume of both loads. Hence, the observations can be written as follows:

$$o_t = \begin{bmatrix} v_1, v_2, v_3, v_4, v_5,\ p, L_L, L_R, P_{cL},\ P_{cR}, P_{lL},\ P_{lR}, \\ \bar{P}_{lL,t},\ \bar{P}_{lR,t}, \bar{P}_{lL,t+1},\ \bar{P}_{lR,t+1}, \bar{P}_{lL,t+2},\ \bar{P}_{lR,t+2}, c_L, c_R \end{bmatrix}. \tag{26}$$

To aid convergence, the observation space is normalized in the range of $[-1, 1]$.

2) Actions: The moveable part position and the states of the five valves can be controlled. The part can move in the continuous workspace $[p_d, p_u]$ depending on the fabrication parameters. Each valve can be opened and closed discretely. Therefore, all actions can be represented as follows:

$$a_t = (p, v_j) \mid p \in [p_d, p_u] \tag{27}$$

$$v_j \in \{0, 1\}, \; j = 0, 1, 2, 3, 4, 5. \tag{28}$$

In each step of an episode, the pump first moves the part to p and then opens and closes the valve v_j. In our implementation, all actions are continuous. To ensure that only one valve is opened at a time, we open the valve corresponding to the highest value within the action vector. If v_0 has the highest value, then no valves are opened

$$j = \operatorname{argmax}(v_1, v_2, \ldots, v_5, v_0). \tag{29}$$

3) Rewards: Our goal is to control the pump to actuate two loads independently such that the load pressures can track two separate target pressures. Depending on applications, these target pressures may be commands issued by higher level controllers for specific tasks. As previously mentioned, sequences of randomly generated target pressures are used during training. The controller aims to choose an optimal action trajectory to minimize loss between target and actuated load pressure in few steps as possible. Therefore, we structure the step reward function as

$$r_t = -\left(\left|\bar{P}_L - P_{lL}\right| + \left|\bar{P}_R - P_{lR}\right|\right) \tag{30}$$

where $\bar{P}$ is the target pressure, and P_{lL} and P_{lR} denote the measured pressures in the left load and right load, respectively. This reward penalizes every step the agent takes weighted by pressure errors, forcing it to choose a possibly short and accurate sequence of actions to reach the target pressure.

For the controller to purposefully change the load pressure, a sequence of several actions must be performed. However, the current state only affects the potential of reward for several future states. Hence, we train our reinforcement-learning agent to maximize cumulative reward within a finite horizon with a discounting factor of $\gamma = 0.92$.

B. Domain Randomization

To increase the robustness of the controller when facing real-world dynamics, we inject random elements within the simulated environment [27], [28]. We first randomize load elastic by a uniform distribution

$$C_d \sim U(0, K_d). \tag{31}$$

The scale of deformation is determined by a hyperparameter K_d. This could mimic the effect of actuating various soft actuators with different stiffness. Besides, random noise is injected within all observations in proportion to the expected range of observations; the SNR ratio of which is determined by a hyperparameter K_n

$$o_t = (1 + C_n)\; o_t, \text{ where } C_n \sim U(0, K_n). \tag{32}$$

A sequence of target pressure for both left and right loads is generated using random combinations of sine, square, and sawtooth waves. Each constituent wave has an amplitude $A_k \sim U(0.3P_0, 3.0P_0)$, period $T \sim U(1\pi,\ 5\pi)$, and phase $\emptyset \sim U(0,\ 2\pi)$. Square and sawtooth waves have a duty cycle of 50%. The resulting target sequence is an average of randomly generated waves.

C. Interactive Load Context Perception

Important parameters of soft actuators, such as initial actuator volume $\hat{V}_l$ and material elastic term C_d, are unknown and cannot be directly measured. However, these features are crucial information for the controller because they affect how air pressure changes when pumping. In this article, we propose to allow the pump to perceive a particular load context by observing the outcomes of specific pumping actions without using extra instruments. The load context can be expressed as a vector

$$c = [\hat{V}_l^0, \hat{C}_d]^T. \tag{33}$$

Specifically, we design an interactive load perception method that automatically conducts perception routines at the start of each episode. We perform a sequence of actions to achieve specific chamber pressures, then equalize load and chamber pressures by opening the corresponding valves between the load and the chamber. Hence, each data point consists of chamber and load pressures before equalization $P_c^{t_1}$ and $P_l^{t_1}$, and the pressure after equalization P^{t_2}. From (12), we obtain a linear equation

$$\frac{P_l^{t_1} - P^{t_2}}{P^{t_2} - P_c^{t_1}} \hat{V}_l^0 - \frac{P_l^{t_1} + P^{t_2} - P_0}{P_0 V_c} \hat{C}_d = 1. \tag{34}$$

We, therefore, can collect n datapoints and solve c using the least square.

This method, combined with domain randomization, enables the agent to be trained entirely in simulation and adapt to the real world quickly without any sim-2-real fine-tuning.

V. Experiments

A. Characterization of Pumping Performance

In this experiment, we examined the real-time pressure and flow rate of the pump. Two pressure sensors (SMC Yadke DP101) were used to measure the air pressure in both chambers and a flowmeter (SMC PFM7) was used to measure instant flow rates. The system setup is shown in Fig. 6.

To validate the pumping performance of the pump, we designed a test trajectory that repeated two example pumping cycles (see Fig. 2) for three iterations. The resulting chamber pressures are shown in Fig. 7. It can be observed that when the moveable part moved to one side, the pressure of the corresponding chamber increased, and the other one decreased as expected. Moreover, with a predefined pumping sequence, the next cycle could attain higher positive or lower negative pressure depending on which pumping sequence is executed. When attempting to attain positive pressure in the left chamber, 103 kPa can be attained after the third iteration. When executing the negative pressure cycle, -44 kPa can be achieved after the third cycle.

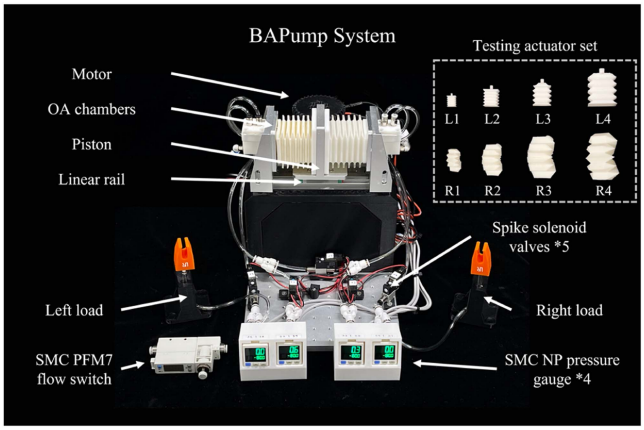

Fig. 6. Experimental system includes an antagonistic pump, pneumatic loads, flow sensors, and pressure sensors. A set of soft pneumatic actuators with different sizes and thicknesses that are used in experiments is shown.

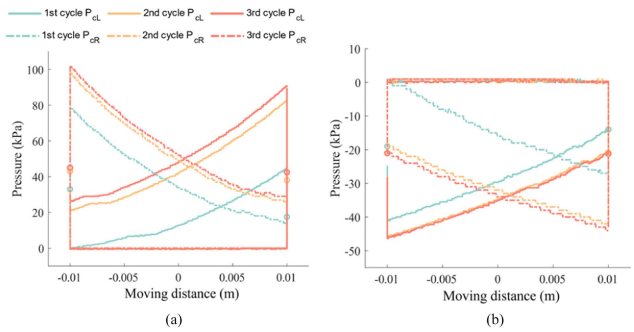

Fig. 7. Characterization of chamber pressure in three pumping iterations without liquid infilling. Lines of different colors represent the first, second, and third iterations. Solid and dot dash lines represent the left and right chamber pressure, respectively. The pumping actions follow the predefined cycles, as shown in Fig. 2. (a) Pressure versus chamber length changing amount at positive pressure range. (b) Pressure versus chamber length changing amount at negative pressure range.

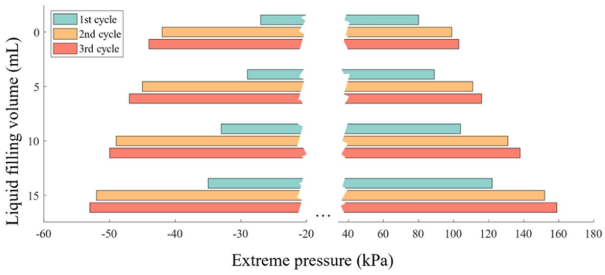

Fig. 8. Extreme pressure versus infilling liquid volume. The pump chambers were infilled with water of 0, 5, 10, and 15 mL. Then, the pump executed the predefined pumping cycles three times.

Second, we tested the extreme pressure the pump system can achieve under different volumes of liquid filling. Precisely, the chamber was filled with 0-mL, 5-mL, 10-mL, and 15-mL water, respectively. Then, three cycles of positive and negative pumping were executed. At the same time, extreme pressures were collected. From the results in Fig. 8, it can be observed that increasing the infilling volume often led to larger extreme pressure. This conclusion can help customize the output pressure range for the universal actuation of various soft robots.

Third, we tested the flow rate performance of the pump. The experimental result is shown in Table I, where a positive value indicates that the airflow direction is from the chamber to the atmosphere and vice-versa.

Although two pumping sequences used in this experiment can, to some extent, control the chamber pressure, we did not use these fixed pumping sequences to actuate soft actuators. Instead, the reinforcement-learning-based controller was used for much better closed-loop control accuracy and much more robust performance when actuating different unseen loads.

B. Pressure Control Performance

Due to the bioinspired nature of the pump, traditional controllers have difficulties controlling the pumping pressure. The designed reinforcement-learning-based controller has two further advantages. First, it can learn and find the optimal action trajectory to the target pressure using as few steps as possible, without predefined action templates. Second, it can adapt to different pneumatic loads using interactive context perception. This allows the pump to actuate various soft robotic actuators robustly without policy fine-tuning on the specific loads.

To train the policy network, we first built an OpenAI Gym [29] simulator using the analytical model ("Methods" section) with parameters tuned against the real pump. The actor network of SAC [30] has a size $(N_o, 64, 64)$ with ReLU and tanh activation. The critic network has a size $(N_o + N_a, 64, 64)$ with ReLU activation, where N_o and N_a are the dimension of observation and action space, respectively. The learning rate for the Adam optimizer [31] was 0.0003 for both networks during training. The algorithm was implemented using Stable-Baselines3 [32] and PyTorch [33]. Training is performed solely in simulation, and testing is both in simulation and the real world. Although the agent has not been trained in the real world, it can adapt to the real world robustly without any fine-tuning, thanks to the interactive load context perception ("Methods" section).

We tested the trained agent to simultaneously control two pneumatic actuators with unknown volume and elasticity, which simulated a hard case in soft robot control. The goal is to control the pressure of loads (P_{lL}, P_{lR}) to track random reference signals $(\bar{P}_{lL}, \bar{P}_{lR}) = \{(\bar{p}^1_{lL}, \bar{p}^1_{lR}), (\bar{p}^2_{lL}, \bar{p}^2_{lR}), \ldots, (\bar{p}^N_{lL}, \bar{p}^N_{lR})\}$, where $N = 100$. Averaged summations of sine, square, and sawtooth waves with random amplitude were used to generate random $\bar{P}_{lL}$ and $\bar{P}_{lR}$.

To evaluate the robustness of pressure control, we used the cumulative reward mean, which was the average loss of pressure error. The agent was trained with unknown small loads, whose volumes were smaller than twice the initial chamber volume. And the agent was tested with a broader range of unknown loads, whose volumes were smaller than eight initial chamber volumes. All loads had random stiffness. Some examples of tracking procedures are shown in Fig. 9. The generalization performance is summarized in Fig. 10(a).

To validate the proposed pressure control method, we performed ablation studies. Agents were trained in five different

TABLE I
PEAK FLOWRATE CHARACTERISTICS (L/MIN)

	First positive cycle	Second positive cycle	Third positive cycle	First negative cycle	Second negative cycle	Third negative cycle
Min	–0.173 ± 0.003	–0.175 ± 0.006	–0.1708 ± 0.004	–0.3333± 0.018	–0.3979± 0.020	–0.4000± 0.017
Max	0.052 ± 0.018	1.1895 ± 0.042	1.2270 ± 0.041	0.3376± 0.006	0.3645± 0.013	0.3584± 0.018

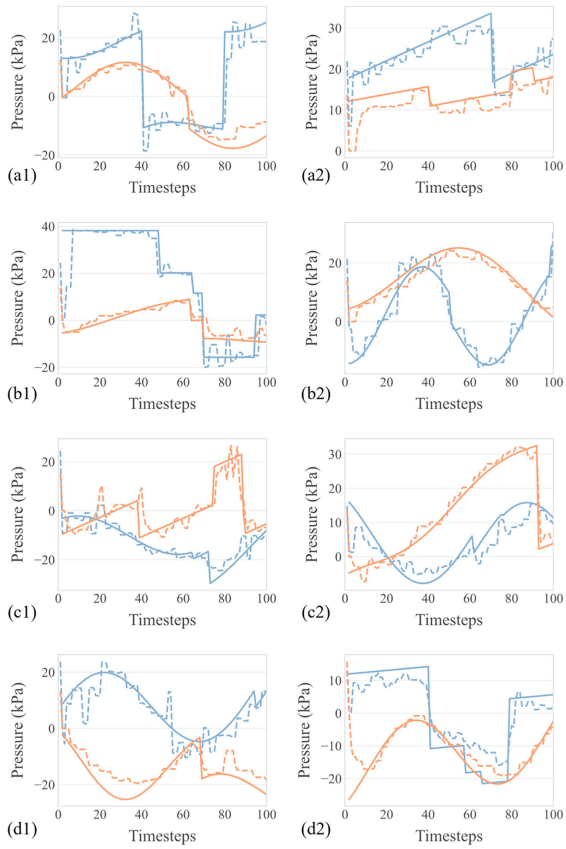

Fig. 9. Performance of the pressure controller on real soft robot actuators. The agent was trained solely in simulation with loads whose volume was within twice the initial chamber volume. Then, the agent was directly tested with unseen loads in real world (see Fig. 6) of sizes 1–4 (a)–(d), whose volume ranges from 0.1 to 1.7 times of the initial chamber volume. Solid lines are the goal pressure of left and right loads, and dashed lines represent the measured pressure.

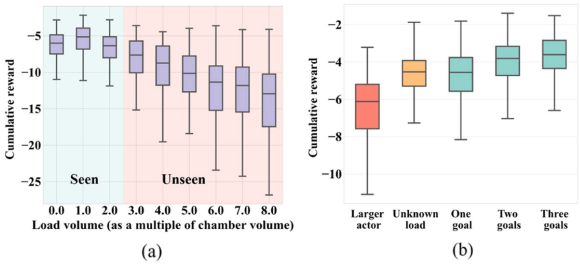

Fig. 10. Generalization and ablation study. (a) Reinforcement-learning-based pressure control generalization on seen and unseen loads in simulation. The agent was trained over small loads and being tested over small and large loads. (b) Ablation study showed that the proposed learning method ("Three goals") achieved the best cumulative reward.

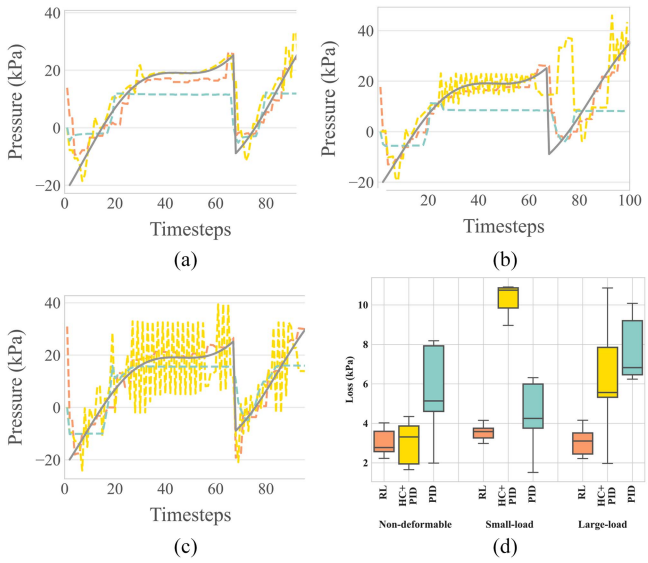

Fig. 11. Comparison with other controllers. Orange represents the RL-based controller (ours), yellow represents the handcrafted PID controller (HC+PID), and cyan represents the PID controller (PID). Gray lines are randomly referenced. (a) Controlling the pressure of nondeformable soft actuators. (b) Controlling the pressure of small soft actuators. (c) Controlling the pressure of large actuators. (d) Mean and standard deviation of seven replicates.

training setups for 10M steps. These training setups are: only the current goal is observable (one goal), the current goal and one future goal are observable (two goals), and the current goal and two future timestep goals are observable (three goals), without performing load context perception (unknown load), using a neural network with a larger size of 256 × 256 (larger actor). The results are shown in Fig. 10(b). Our proposed method achieves the best performance. It was also noticed that the proposed load context perception could effectively mitigate the impact of unknown loads. However, a larger network did not result in lower loss.

We compared the proposed pressure control method with other traditional controllers. Regarding tracking pressures in both left and right loads, there is no straightforward method of designing a handcrafted controller for such a task. Therefore, the reinforcement learning (RL)-based controller is the clear winner in this case. For comparison with other types of controllers, we handicap the difficulty of the challenge by only tracking the pressures of a single load.

First, a PID controller is tuned to control the movement of the piston to track pressure goals within a single cycle of the

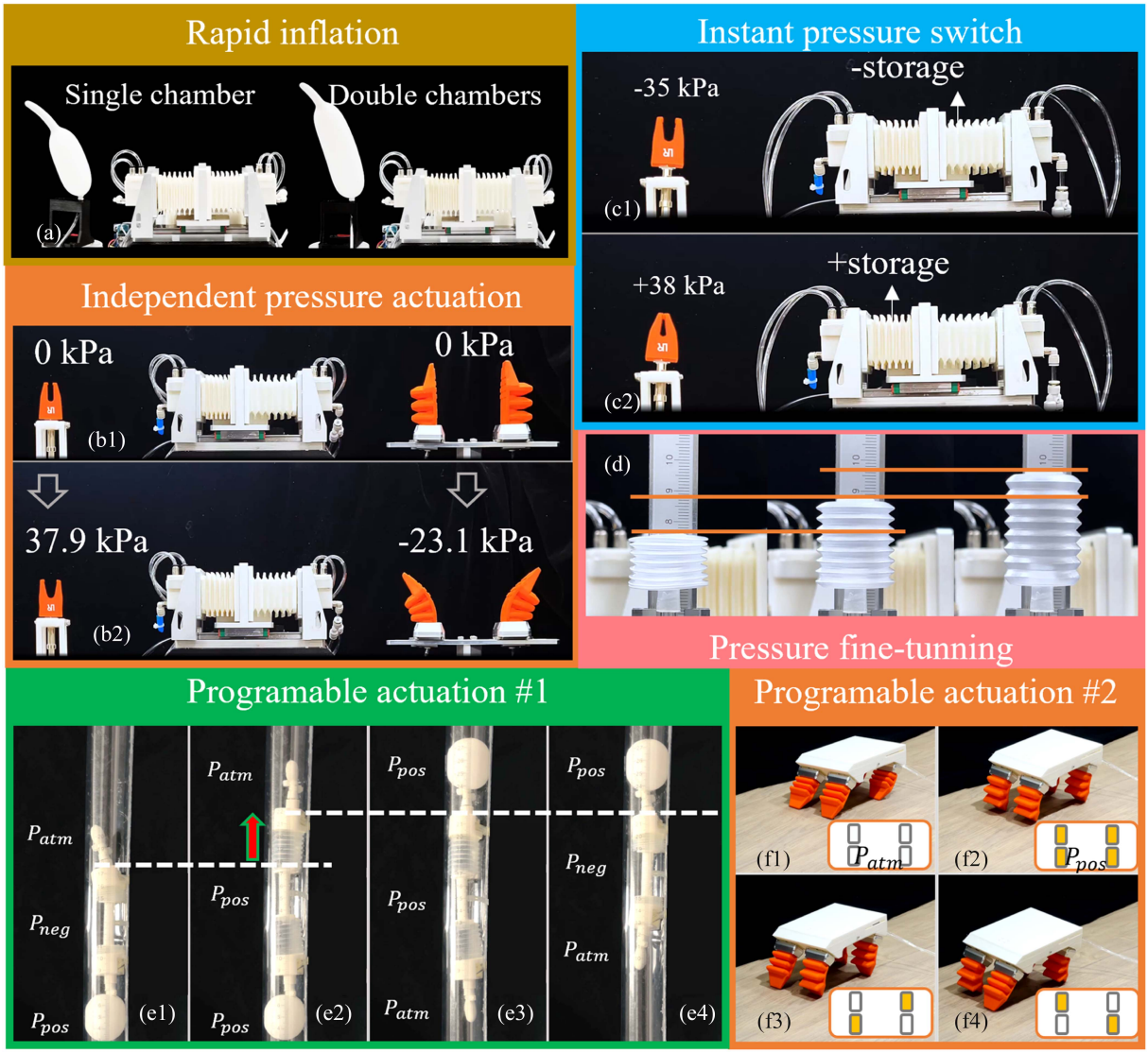

Fig. 12. Application demonstrations. (a) Balloon inflation by double-chamber pumping compared with single-chamber pumping. The former has higher efficiency. (b1) and (b2) Simultaneously and independently controlling the pressure of two soft robotic grippers. (c1) and (c2) Instant switch from -35 to $+38$ kPa. (d) Precise pressure fine-tuning using the moveable part. (e1)–(e3) Crawling robot locomotion demonstration. The head, foot, and body of the crawling robot were controlled by the pump in a certain way such that it was moving upward inside a tube. (f1)–(f4) Turtle robot locomotion demonstration. Four legs of the turtle robot were actuated by the pump in a certain order.

pump for a load size equivalent to 0.8 of chamber volume. Rule-based heuristics are then hard coded into another handcrafted controller to the best of our efforts to operate the pump for multiple cycles to achieve large positive/negative pressures while using the PID controller to track small changes within a single cycle. Finally, the proposed RL-based controller is tested without further fine-tuning.

The 63 pressure tracking experiments are conducted with combinations of the three controllers (RL, handcrafted PID, and PID) and three types of loads (nondeformable, small-deformable, and large-deformable actuators) and seven replicates. The results are shown in Fig. 11.

RL performs similarly for all three cases. This is expected since RL was trained on all these cases via domain randomization and interactive load context perception. The handcrafted controller performs well in the task tuned on (nondeformable load) but performs poorly in other unseen cases. When it comes to pumping large positive/negative pressures, handcrafted routines can be hard coded (instead of being learned as a long-horizon sequence in RL). However, despite our best efforts, the handcrafted routine is still imperfect for such a difficult task. The simple PID control is also not designed for nonlinear systems, such as air pressure. For the PID controller, since PID controllers only work on continuous tracking and cannot determine when to execute discrete actions, such as opening valves, they cannot achieve pressures that are beyond a single cycle, thus ensuring that they would fail to achieve large positive or negative pressures.

C. Application Demonstrations

In total, six demonstrations were presented: pneumatic actuation of soft actuators, continuous pressure tuning, instant pressure switch, balloon inflation, turtle robot locomotion, and crawling robot locomotion.

First, we combined two-chamber outputs together into one outlet and then connected a balloon to the combined outlet. In this way, the proposed system sacrificed the ability to actuate multiple loads but can perform rapid inflation, as shown in Fig. 12(a). We compared two cases: using a single chamber and using double chambers. When using a single chamber to pump, the pump blew gas when the stroke was in one direction and refilled the chamber in the other direction, which was not efficient. While using double chambers, the pump can expel gas during both strokes; therefore, in this case, the pump completed the task using less strokes.

Second, the pump kept the former connection and performed an instant pressure switch, as shown in Fig. 12(c1) and (c2). In this demonstration, the pump first controlled the pressure of one chamber to a pressure level (positive in this demonstration) and the other chamber to another pressure level (negative in this demonstration). Then, the pump opened the valve between the chamber with positive pressure and the soft gripper. Instantly, the soft gripper fingers opened because of the positive pressure. To quickly switch pressure to zero and even negative, the pump system opened the valve connecting the atmosphere and the chamber with positive pressure, driving the soft gripper to the neutral pose. Instantly, the pump system closed previously opened valves and opened the valve that connected the chamber with negative pressure and the soft gripper, driving the gripper to the closing state with negative pressure. It should be noted that the pump can instantly switch between any two pressure states within the working range. This demonstrated that the proposed pump system could fast switch between positive and negative pressure outputs, which was helpful for actuating soft robots that have discrete states.

Third, we connected one linear soft actuator to the chamber output and used the pump system to fine-tune the end position of the soft actuator, as shown in Fig. 12(d). It was achieved by freezing valve actions and only allowing chamber movements. This function makes it possible to precisely adjust, for example, the fingertip position of a soft robotic hand for some manipulation tasks.

Fourth, we connected one soft gripper to the left chamber output and one soft finger of a different type to the right chamber output, by which the pump can simultaneously actuate two soft robot actuators. We then commanded the pump system to increase the pressure of one load and decrease the pressure of the other, as shown in Fig. 12(b1) and (b2). This demonstrated that the proposed pump system could actuate one or two different soft robot actuators or soft robots with one to two degrees of freedom. By combining more pumps, soft robots with more degrees of freedom can be actuated.

Finally, we used the pump to control two different soft locomotion robots to demonstrate its versatile pumping ability. Fig. 12(e1)–(e4) presents a soft climbing robot actuated by the pump to climb a tube. Fig. 12(f1)–(f4) presented a turtle robot walking demonstration. Each time, the pump actuated two legs of the turtle robot with positive pressure. The leg will bend under positive pressure and relax under atmospheric pressure.

VI. Conclusion

This study presents an innovative bioinspired antagonistic pump that emulates the anatomical structure of fish hearts, thereby enabling programmable pneumatic actuation and adaptive control of diverse pneumatic soft robots. The research encompasses the design, modeling, and fabrication of a prototype pump capable of regulating pressure within the range of -44 to $+103$ kPa (-52 to $+159$ kPa with maximum liquid infilling) and achieving a peak flow rate of 1.2 L/min, which is suitable for driving pneumatic soft robots [34], [35], [36]. The designed pump has multiple pumping modes, including unknown load perception, rapid inflation, double-load control, adaptive pumping across positive and negative pressure ranges, precise fine-tuning, and instant pressure switches.

Leveraging the unique attributes of the pump, a reinforcement-learning-based pressure control algorithm is developed for precise pneumatic output pressure regulation. Moreover, an interactive load context perception method is devised to intelligently adapt pumping strategies without knowing the soft robot properties as a prior, facilitating the universal actuation of soft robots. Notably, the learning-based controller can be trained in simulation and directly applied in real-world scenarios without necessitating fine-tuning.

To further enhance the understanding of the pump's structural characteristics, future endeavors will encompass a finite-element method-based structural analysis. Furthermore, the research aims to employ advanced material as pump actuators and soft valves, which will aim to shrink the volume of the pump system and apply to untethered actuation applications. In addition, the study intends to explore flow rate controllers alongside pressure controllers, thereby broadening the applicability [37], [38], [39], [40], [41], [42], [43] of the proposed technology in various scenarios.

References

[1] J. Walker et al., "Soft robotics: A review of recent developments of pneumatic soft actuators," *Actuators*, vol. 9, no. 1, Mar. 2020, Art. no. 3, doi: 10.3390/act9010003.

[2] H. Cao, J. Huang, Y. Li, J. Zhou, and Y. Liu, "Fuzzy-depth objects grasping based on FSG algorithm and a soft robotic hand," in *Proc. IEEE/RSJ Int. Conf. Intell. Robots Syst.*, 2021, pp. 3948–3954.

[3] Y. Li et al., "Untethered multimode fluidic actuation: A new approach to soft and compliant robotics," *Soft Robot.*, vol. 8, no. 1, pp. 71–84, Feb. 2021, doi: 10.1089/soro.2019.0131.

[4] J. Zhou, Y. Li, Y. Yang, H. Cao, J. Huang, and Y. Liu, "A 22-DOFs bio-inspired soft hand achieving 6 kinds of in-hand manipulation," in *Proc. IEEE Int. Conf. Real-Time Comput. Robot.*, 2021, pp. 20–26, doi: 10.1109/RCAR52367.2021.9517366.

[5] H. I. Ali, "A review of pneumatic actuators (modeling and control)," *Australian J. Basic Appl. Sci.*, vol. 3, no. 2, pp. 440–454, 2009.

[6] J. Zhou, S. Chen, and Z. Wang, "A soft-robotic gripper with enhanced object adaptation and grasping reliability," *IEEE Robot. Autom. Lett.*, vol. 2, no. 4, pp. 2287–2293, Oct. 2017.

[7] D. B. Parker, "Positive displacement pumps—Performance and application," in *Proc. 11th Int. Pump Users Symp.*, 1994, pp. 1–5, doi: 10.21423/R10T29.

[8] Q. He and S. Cai, "Soft pumps for soft robots," *Sci. Robot.*, vol. 6, no. 51, Feb. 2021, Art. no. eabg6640, doi: 10.1126/scirobotics.abg6640.

[9] D. A. Bettex, R. Pretre, and P.-G. Chassot, "Is our heart a well-designed pump? The heart along animal evolution," *Eur. Heart J.*, vol. 35, no. 34, pp. 2322–2332, Sep. 2014, doi: 10.1093/eurheartj/ehu222.

[10] C. R. Monk, "The anatomy and life-history of a freshwater mollusk of the genus sphaerium," *J. Morphol.*, vol. 45, no. 2, pp. 473–503, 1928, doi: 10.1002/jmor.1050450204.

[11] A. Yamauchi, "Fine structure of the fish heart," *Comp. Anatomy Develop.*, vol. 9, pp. 119–148, 1980.

[12] B. Jensen, T. Wang, V. M. Christoffels, and A. F. Moorman, "Evolution and development of the building plan of the vertebrate heart," *Biochimica et Biophysica Acta -Mol. Cell Res.*, vol. 1833, no. 4, pp. 783–794, 2013.

[13] T. A. Riemenschneider and A. J. Moss, "Left ventricular—Right atrial communication," *Amer. J. Cardiol.*, vol. 19, no. 5, pp. 710–718, 1967.

[14] F. Torrent-Guasp et al., "Towards new understanding of the heart structure and function," *Eur. J. Cardio-Thoracic Surg.*, vol. 27, no. 2, pp. 191–201, Feb. 2005, doi: 10.1016/j.ejcts.2004.11.026.

[15] A. J. Clark, *Comparative Physiology of the Heart*. Cambridge, U.K., MA, USA: Cambridge Univ. Press, 2015.

[16] P. Laurent, S. Holmgren, and S. Nilsson, "Nervous and humoral control of the fish heart: Structure and function," *Comp. Biochem. Physiol. A, Physiol.*, vol. 76, no. 3, pp. 525–542, Jan. 1983, doi: 10.1016/0300-9629(83)90455-3.

[17] S. J. Crick, M. N. Sheppard, S. Y. Ho, L. Gebstein, and R. H. Anderson, "Anatomy of the pig heart: Comparisons with normal human cardiac structure," *J. Anatomy*, vol. 193, no. 1, pp. 105–119, Jul. 1998, doi: 10.1046/j.1469-7580.1998.19310105.x.

[18] P. J. Hunter, A. D. McCulloch, and H. E. D. J. ter Keurs, "Modelling the mechanical properties of cardiac muscle," *Prog. Biophys. Mol. Biol.*, vol. 69, no. 2/3, pp. 289–331, Mar./May 1998, doi: 10.1016/S0079-6107(98)00013-3.

[19] H. Fukuta and W. C. Little, "The cardiac cycle and the physiologic basis of left ventricular contraction, ejection, relaxation, and filling," *Heart Failure Clinic*, vol. 4, no. 1, pp. 1–11, Jan. 2008, doi: 10.1016/j.hfc.2007.10.004.

[20] C. Knospe, "PID control," *Control Syst. Mag.*, vol. 26, no. 3, pp. 30–31, Mar. 2006, doi: 10.1109/MCS.2006.1580151.

[21] M. L. Darby and M. Nikolaou, "MPC: Current practice and challenges," *Control Eng. Pract.*, vol. 20, no. 4, pp. 328–342, Apr. 2012, doi: 10.1016/j.conengprac.2011.12.004.

[22] J. Huang et al., "Modular origami soft robot with the perception of interaction force and body configuration," *Adv. Intell. Syst.*, vol. 4, no. 9, 2022, Art. no. 2200081, doi: 10.1002/aisy.202200081.

[23] D. Bach, F. Schmich, T. Masselter, and T. Speck, "A review of selected pumping systems in nature and engineering—Potential biomimetic concepts for improving displacement pumps and pulsation damping," *Bioinspiration Biomimetics*, vol. 10, no. 5, Sep. 2015, Art. no. 051001, doi: 10.1088/1748-3190/10/5/051001.

[24] "High flow, high pressure, double acting, dual piston air driven liquid pump, series AHL66-2D on parker/autoclave engineers FCD," *Parker/Autoclave Engineers FCD*, Accessed on: Jun. 14, 2023. [Online]. Available: https://parker.autoclave.com/viewitems/compact-hand-lever-liquid-pumps/dual-piston-air-driven-liquid-pump-series-ahl66-2d

[25] S. A. Sakhare et al., "Design suggestions on modified self-sustainable space toilet," *SN Appl. Sci.*, vol. 4, Jan. 2022, Art. no. 13, doi: 10.1007/s42452-021-04878-w.

[26] M. L. Puterman, "Chapter 8 Markov decision processes," in *Handbooks in Operations Research and Management Science*, vol. 2. Amsterdam, The Netherlands: Elsevier, 1990, pp. 331–434, doi: 10.1016/S0927-0507(05)80172-0.

[27] J. Tobin, R. Fong, A. Ray, J. Schneider, W. Zaremba, and P. Abbeel, "Domain randomization for transferring deep neural networks from simulation to the real world," in *Proc. IEEE/RSJ Int. Conf. Intell. Robots Syst.*, 2017, pp. 23–30, doi: 10.1109/IROS.2017.8202133.

[28] J. Tobin et al., "Domain randomization and generative models for robotic grasping," 2018, Accessed on: Nov. 1, 2020. [Online]. Available: http://arxiv.org/abs/1710.06425

[29] G. Brockman et al., "OpenAI gym," Jun. 5, 2016, Accessed on: Feb. 1, 2023. [Online]. Available: http://arxiv.org/abs/1606.01540

[30] T. Haarnoja et al., "Soft actor-critic algorithms and applications," Jan. 29, 2019, Accessed on: Feb. 1, 2023. [Online]. Available: http://arxiv.org/abs/1812.05905

[31] S. Bock and M. Weiß, "A proof of local convergence for the Adam optimizer," in *Proc. IEEE Int. Joint Conf. Neural Netw.*, 2019, pp. 1–8, doi: 10.1109/IJCNN.2019.8852239.

[32] A. Raffin, A. Hill, A. Gleave, A. Kanervisto, M. Ernestus, and N. Dormann, "Stable-baselines3: Reliable reinforcement learning implementations," *J. Mach. Learn. Res.*, vol. 22, no. 268, pp. 1–8, 2021.

[33] A. Paszke et al., "PyTorch: An imperative style, high-performance deep learning library," in *Proc. 33rd Int. Conf. Neural Inf. Process. Syst.*, 2019, Accessed on: Oct. 8, 2022. [Online]. Available: https://proceedings.neurips.cc/paper/2019/hash/bdbca288fee7f92f2bfa9f7012727740-Abstract.html

[34] F. Connolly, P. Polygerinos, C. J. Walsh, and K. Bertoldi, "Mechanical programming of soft actuators by varying fiber angle," *Soft Robot.*, vol. 2, no. 1, pp. 26–32, Mar. 2015, doi: 10.1089/soro.2015.0001.

[35] D. Yang et al., "Buckling of elastomeric beams enables actuation of soft machines," *Adv. Mater.*, vol. 27, no. 41, pp. 6323–6327, Nov. 2015, doi: 10.1002/adma.201503188.

[36] F. Ilievski, A. D. Mazzeo, R. F. Shepherd, X. Chen, and G. M. Whitesides, "Soft robotics for chemists," *Angewandte Chemie*, vol. 123, no. 8, pp. 1930–1935, Feb. 2011, doi: 10.1002/anie.201800907.

[37] H. Cao, W. Chen, Y. Lu, J. Huang, J. Zhou, and Y. Liu, "An end-to-end proprioception framework for soft continuum robot," in *Proc. IEEE Int. Conf. Robot. Biomimetics*, 2022, pp. 141–147, doi: 10.1109/ROBIO55434.2022.10011982.

[38] J. Zhou, H. Cao, W. Chen, S. S. Cheng, and Y.-H. Liu, "Bioinspired soft wrist based on multicable jamming with hybrid motion and stiffness control for dexterous manipulation," *IEEE/ASME Trans. Mechatron.*, vol. 28, no. 3, pp. 1256–1267, Jun. 2023, doi: 10.1109/TMECH.2022.3224183.

[39] W. Chen et al., "Tele-operated oropharyngeal swab (TOOS) robot enabled by TSS soft hand for safe and effective sampling," *IEEE Trans. Med. Robot. Bionics*, vol. 3, no. 4, pp. 1040–1053, Nov. 2021, doi: 10.1109/TMRB.2021.3123530.

[40] J. Zhou et al., "A soft-robotic approach to anthropomorphic robotic hand dexterity," *IEEE Access*, vol. 7, pp. 101483–101495, 2019, doi: 10.1109/ACCESS.2019.2929690.

[41] J. Zhou, J. Yi, X. Chen, Z. Liu, and Z. Wang, "BCL-13: A 13-DOF soft robotic hand for dexterous grasping and in-hand manipulation," *IEEE Robot. Autom. Lett.*, vol. 3, no. 4, pp. 3379–3386, Oct. 2018, doi: 10.1109/LRA.2018.2851360.

[42] H. Cao et al., "Two-stage grasping: A new bin picking framework for small objects," in *Proc. IEEE Int. Conf. Robot. Autom.*, 2023, pp. 2584–2590, doi: 10.1109/ICRA48891.2023.10160608.

[43] K. Chin, T. Hellebrekers, and C. Majidi, "Machine learning for soft robotic sensing and control," *Adv. Intell. Syst.*, vol. 2, no. 6, Jun. 2020, Art. no. 1900171, doi: 10.1002/aisy.201900171.

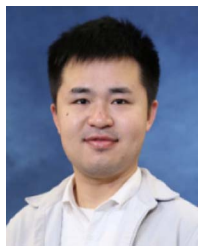

Jianshu Zhou (Member, IEEE) received the Ph.D. degree in mechanical engineering from the Department of Mechanical Engineering, The University of Hong Kong, Hong Kong, in 2020.

He is currently a Research Assistant Professor with The Chinese University of Hong Kong, Hong Kong, after his postdoctoral research with the same department. His research interests include robotics, grasping and manipulation, soft robotics, and robotic hands.

Wei Chen received the B.E. degree in computer science and technology from Zhengzhou University, Zhengzhou, China, in 2012, and the M.S. degree in mechanical and automation engineering in 2021 from the Chinese University of Hong Kong, Hong Kong, where he is currently working toward the Ph.D. degree in mechanical and automation engineering.

His research interests include soft robotics and medical robots.

Hanwen Cao (Graduate Student Member, IEEE) received the B.S. degree in measuring and control technology and instruments from Tianjin University, Tianjin, China, in 2017, M.E. degree in instrument science and technology from Tianjin University, Tianjin, China, in 2020, and the M.S. degree in electrical and computer engineering from the Georgia Institute of Technology, Atlanta, GA, USA, in 2020. He is currently working toward the Ph.D. degree in mechanical and automation engineering with the Chinese University of Hong Kong, Hong Kong.

His research interests include soft robotic grasping.

Qiguang He received the B.S. degree in mechanical engineering from Tsinghua University, Beijing, China, in 2015, and the M.S. and Ph.D. degrees in mechanical engineering from the University of California, San Diego, CA, USA, in 2017 and 2021, respectively.

After working with the University of Pennsylvania as a Postdoctoral Researcher, he joined The Chinese University of Hong Kong, as an Assistant Professor, in 2023. His research interests include soft robotics, smart materials, and additive manufacturing.

Yunhui Liu (Fellow, IEEE) received the B.Eng. degree from the Beijing Institute of Technology, Beijing, China, in 1985, the M.Eng. degree from Osaka University, Osaka, Japan, in 1989, and the Ph.D. degree in mathematical engineering from the University of Tokyo, Tokyo, Japan, in 1992.

In 1995, he joined The Chinese University of Hong Kong (CUHK), where he is currently a Choh-Ming Li Professor of mechanical and automation engineering and the Director of the CUHK T Stone Robotics Institute. He is also an Adjunct Professor with the State Key Laboratory of Robotics Technology and System, Harbin Institute of Technology, Harbin, China. He has authored or coauthored more than 300 articles in refereed journals and refereed conference proceedings and was listed in the Highly Cited Authors (Engineering) by Thomson Reuters in 2013. His research interests include visual servoing, medical robotics, multifingered grasping, mobile robots, and machine intelligence.